Wall heat loads in a cryogenic rocket thrust chamber during thermoacoustic instabilities

Govaert, Thomas; Armbruster, Wolfgang; Hardi, Justin S.; Suslov, Dmitry; Oschwald, Michael; Zandbergen, Barry T.C.

DOI
10.2514/1.B38304

Publication date
2021

Document Version
Final published version

Published in
Journal of Propulsion and Power

JOURNAL OF PROPULSION AND POWER
Vol. 37, No. 6, November–December 2021

Wall Heat Loads in a Cryogenic Rocket Thrust Chamber During Thermoacoustic Instabilities

Thomas Govaert*
Aerospace Propulsion Products, 4791 RT Klundert, The Netherlands
Wolfgang Armbruster,† Justin S. Hardi,‡ Dmitry Suslov,§ and Michael Oschwald¶
DLR, German Aerospace Center, 74239 Hardthausen, Germany
and
Barry T. C. Zandbergen**
Delft University of Technology, 2629 HS Delft, The Netherlands

https://doi.org/10.2514/1.B38304

A subscale, research rocket thrust chamber operating with cryogenic oxygen and hydrogen exhibits self-excited transverse-mode instabilities with amplitudes of more than 80% of the steady combustion chamber pressure (peak-to-peak) for some operating conditions. During unstable combustion, an increase in the integral heat flux into the water-cooled combustion chamber walls of 20–40% with respect to stable conditions was experienced. A model was derived to predict changes in the axial heat flux profile considering only the dependence of flame length on the amplitude of transverse acoustic oscillations. The model predicts an increase in heat flux in the upstream part of the chamber by up to a factor of 7. This drastic increase is in agreement with past observations of rocket engine failures due to instabilities, in which the structural damage is commonly observed on the faceplate and the walls adjacent to the injection plane. The model also predicts a peak increase in integral heat flux of up to about 25%. While falling short of the peak experimental value of 40%, it nevertheless suggests that flame length is the dominant influence on the distribution of thermal loads in this study.

Nomenclature

D	=	diameter, m
f	=	frequency, Hz
H	=	enthalpy, J
h	=	specific enthalpy, J/kg
L	=	length, m
$\dot{m}$	=	mass flow, kg/s
p	=	pressure, bar
$\dot{Q}$	=	heat flow, W
$\dot{q}$	=	heat flux, W/m^2
ROF	=	ratio of oxidizer to fuel mass flow
T	=	temperature, K
t	=	time, s
u	=	velocity, m/s
x	=	axial distance from injection plane, m
ρ	=	density, kg/m^3
ϕ	=	phase, rad
ω	=	angular velocity, rad/s

Subscripts

c	=	sonic
CC	=	completed combustion
cc	=	combustion chamber
eff	=	effective
HG	=	hot gas
int	=	integrated
pred	=	predicted
sc	=	sensor cooling
T	=	first transverse acoustic mode
w	=	chamber wall
%	=	percentage relative change

I. Introduction

ONE of the most challenging problems encountered in the development of liquid propellant rocket engine (LPRE) thrust chambers is high-frequency combustion instabilities. High-frequency combustion instabilities are oscillations in combustion chamber pressure of a magnitude larger than 10% peak-to-peak of the mean chamber pressure and are generated and sustained by unsteady heat release coupled with chamber acoustic modes [1,2]. Historically, these instabilities have been extremely dangerous for rocket engines, with the most dangerous aspect being an increased heat flux during unstable combustion, which can lead to thermal damage of the injector faceplate or chamber walls, often resulting in mission failure [3–6].

Sutton and Biblarz report observed increases of heat flux between 4 to 10 times that during stable combustion [1], although not differentiating whether this increase was local or integral over the entire chamber length. Similarly, Harrje and Reardon report observed four-fold increases in heat flux during transverse-mode instabilities and smaller increases for longitudinal-mode instabilities [6]. Also, Dranovsky reports heat flux increases of up to a factor of 6, although in this case, observations are focused on heat fluxes near the injector face [5]. Direct experimental measurements have been published by Hulka and Jones, showing increases in heat flux near the injector face up to a factor of 8–12, while the increase in integral heat flux was much less [7]. Some subscale experimental thrust chambers showed

Received 30 October 2020; revision received 14 April 2021; accepted for publication 15 April 2021; published online Open Access 23 June 2021.

*Project Engineer; t.govaert@appbv.nl.
†Topic Leader, Combustion Instabilities, Institute of Space Propulsion; Wolfgang.Armbruster@dlr.de.
‡Head of Rocket Propulsion Technology Department, Institute of Space Propulsion; Justin.Hardi@dlr.de. Senior Member AIAA.
§Team Leader, Thrust Chamber Technology, Institute of Space Propulsion; Dmitry.Suslov@dlr.de. Senior Member AIAA.
¶Coordinator for Rocket Propulsion, Institute of Space Propulsion; currently Institute of Jet Propulsion and Turbomachinery, RWTH Aachen University, 52062 Aachen, Germany; also Professorship for Space Propulsion, Institute of Jet Propulsion and Turbomachinery; oschwald@ist.rwth-aachen.de, Michael.Oschwald@dlr.de. Member AIAA.
**Senior Lecturer, Space Systems Engineering, Faculty of Aerospace Engineering, Kluyverweg 1; b.t.c.zandbergen@tudelft.nl.

significant damage at or close to the injector faceplate, for example failed baffles [8], after combustion instabilities have been observed, while other segments in the chamber remain unaffected. Similar observations have been reported globally, where the presence of high-frequency combustion instabilities causes the injector plate or chamber walls close to the injection plane to often show the most severe damage rather than similar damages throughout the complete combustion chamber length [6,9–11].

Although thermal damage to the upstream region of the combustion chamber has been a known effect of combustion instabilities for decades, there are currently no accepted physical explanations for why these increases of heat flux result from the acoustic oscillations in the chamber. There are some studies that attempt to explain the increased heat transfer through an increase in heat transfer coefficient. A first cause for this could be the destruction of a thermal boundary layer at the chamber wall due to the violent acoustic oscillations [12]. Experimental research on pulse combustors reports only slight to no effect of pressure waves on heat flux to the chamber walls [13,14]. Van Buren and Polifke analyzed the heat transfer coefficient increase due to boundary layer interaction within oscillatory channel flow. The authors reported that there is no enhancement in heat transfer coefficient for laminar flows [15]. However, for turbulent flows, the heat transfer normal to the wall can approximately double for acoustic velocity amplitudes that reach more than four times the convective velocity in the channel [15]. From Bartz's work, it can be seen that the heat transfer coefficient is proportional to convective velocity to the power 0.8, meaning at least a similar factor increase in convective velocity would be required to explain the large heat flux increases [16]. An estimate made in this study shows that a superposition of acoustic velocity on mean flow in the chamber can conceivably increase the local convective velocity to such levels. This effect will appear only locally depending on the distribution of the unstable acoustic mode. Although some increase in local heat transfer coefficient is thus likely, there is still a large gap with respect to reported local increases in heat flux. Therefore, in this study, it is assumed that, although the disturbance of the boundary layer during instabilities might be present and can contribute to the rise of heat flux through an enhancement in heat transfer coefficient, the effect is not strong enough to explain a large part of the reported heat flux increases of orders of magnitude.

Instead, this study focuses on a different and separate aspect, that being a change in flame length and corresponding hot gas distribution over the length of a combustion chamber. From numerical and experimental studies that visualize the response of shear coaxial flames to transverse acoustic oscillations, it is known that the liquid oxygen (LOX) core and the surrounding flame shorten significantly at high amplitude [17–23]. This change in LOX core and flame characteristics influences the heat release distribution within the combustion chamber, but the role of this effect has not yet been explored in accounting for heightened upstream heat flux. The present work addresses this effect in studying the relationship between heat flux and acoustic amplitude in a subscale LOX–hydrogen (H_2) thrust chamber. The chamber showed self-excited, high-amplitude combustion instabilities while operating under conditions highly representative of upper-stage engines [24]. Making use of a water-cooled cylindrical chamber segment, it was possible to determine the total heat flow spatially integrated over the inner wall surface. During transverse-mode combustion instabilities with peak-to-peak amplitudes of more than 80% with respect to the mean combustion chamber pressure, the integral heat flux increased by 10–40%. This observation seems to be inconsistent with the order-of-magnitude increases reported in literature.

This paper presents a new model of heat flux distribution with dependence on the amplitude of transverse combustion instabilities. Applied to the aforementioned thrust chamber, the model can explain both the rather low increase in total heat flow and the significantly higher localized increases of heat flux similar to the values reported in literature.

This paper is structured as follows. First the experimental setup is introduced. Then the determination of increases in heat flux during unstable combustion will be explained. Next, the new model for predicting the redistribution of heat flux is derived in detail. The model is then compared with the experimental results.

II. Experimental Method

A. Subscale Thrust Chamber Model D

The experimental analysis and the derived model have been evaluated with data from the DLR research thrust chamber model D (BKD). The thrust chamber consists of the injector head, an instrumented measurement ring, a cylindrical chamber segment, and a convergent–divergent nozzle, as illustrated in Fig. 1. The inner diameter of the chamber is 80 mm, and the length of the cylindrical part of the chamber is 215.5 mm. The nozzle diameter is 50 mm, yielding a realistic contraction ratio of 2.56 and a characteristic chamber length of $L^* = 0.64$ m. The injector head consists of 42 shear coaxial injection elements with recessed and tapered LOX posts of inner diameter 3.6 mm. The injectors are arranged in three concentric circles, and the corresponding injector pattern is presented in Fig. 2.

To measure the acoustic pressure oscillations, the combustion chamber has been equipped with eight high-frequency pressure sensors. These water-cooled sensors are flush mounted in a measurement ring, which is installed between the injector head and the cylindrical segment as shown in Fig. 1. The signals are recorded with a sampling frequency of 100 kHz, and a 30 kHz antialiasing low-pass filter is applied. The measurement range is set to ± 30 bar. For stable operation with low oscillation amplitudes, a measurement uncertainty of ± 0.054 bar was estimated. For elevated oscillation amplitudes during unstable operation, this value increases to about ± 0.092 bar.

B. Operating Conditions

BKD is operated at the European research and technology test bench P8 for high-pressure combustion. Measurements from several test campaigns covering a wide range of operating conditions with the propellant combination LOX/H_2 are analyzed in this study. The typical LOX injection temperature is about $T_{O_2} = 110$ K, and $T_{H_2} = 95$–100 K. Within the combustion stability research of Grönning et al. [25–27], the combustion chamber pressure p_{cc} was varied between 50 and 80 bar. Thus, all the operating conditions are characterized by transcritical injection. The oxidizer to fuel propellant mixture ratio ($ROF = \dot{m}_{O_2}/\dot{m}_{H_2}$) was varied in the range from 2 to 7. At the load point of $p_{cc} = 80$ bar and $ROF = 6$, the thrust is about 24 kN, and the thermal power is almost 90 MW, which makes BKD comparable to small upper-stage engines.

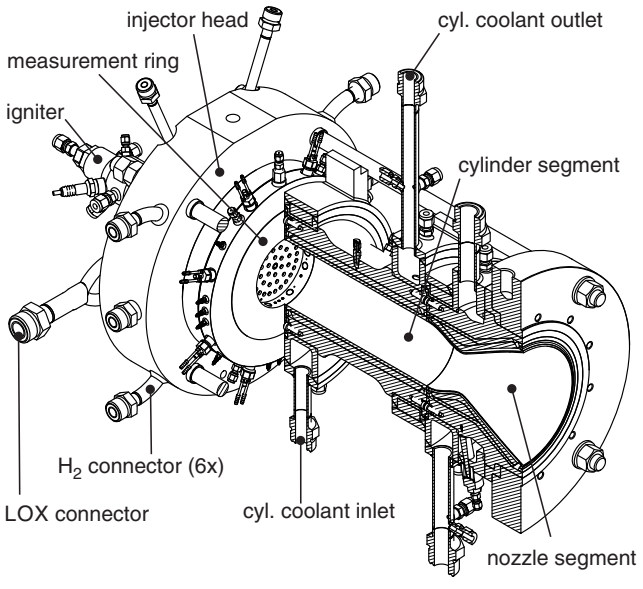

Fig. 1 DLR research thrust chamber BKD.

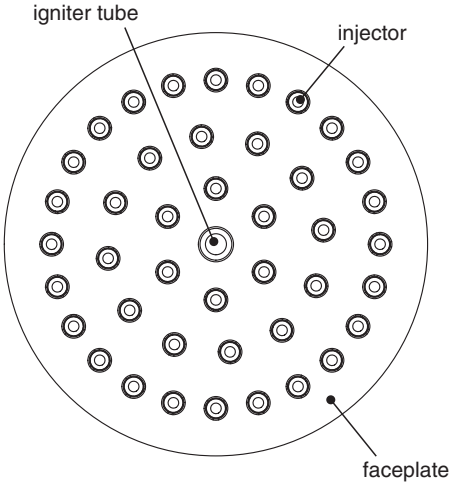

Fig. 2 Injector pattern of BKD [25].

C. Heat Flow Measurements

Originally, the BKD combustor was designed to investigate the heat transfer under regenerative cooling with cryogenic coolants [28]. The liner of the cylindrical segment and the nozzle segment is a copper alloy liner with 95 milled cooling channels. A galvanic nickel jacket closes the cooling channels to the outside. For the investigation of combustion instabilities, the combustion chamber and nozzle segment are water cooled in a coflow direction. Turbine flow meters for each cooled segment measure the mass flow rate of the coolant. Thermocouples and pressure sensors are installed at the inlet and outlet pipes of the cooling circuit in order to measure the pressure drop and temperature rise of the coolant. This allows the increase in enthalpy of the coolant in the chamber segment to be calculated and, hence, the integral heat flux into the chamber walls over the length of both the cylindrical segment and the nozzle segment.

The uncertainty of the experimentally measured heat flow into the cylindrical combustion chamber has been estimated as follows. The measurement accuracy of the temperature difference between thermocouples at the inlet and outlet depends on the total temperature difference and, therefore, on the total heat flow. For the heat flow in the cylindrical segment, the uncertainty is estimated to be less than 12% for 700 kW and below 4% for 2000 kW, corresponding to the bottom and upper limits of measured heat flows.

Losses from the cylindrical segment were also estimated. Radiation losses from the outer surface area of the segment are below 0.1% and are therefore negligible. There is the potential for heat transfer between the contacting surfaces of the warm end of the cylindrical segment and the colder front face of the nozzle segment. Based on the temperature difference of the coolant water between cylinder exit and nozzle inlet, the distance between the inlet and outlet cooling channels, and the thermal conductivity of the liner material and the contact area, the axial enthalpy losses from the cylinder into the nozzle have been conservatively estimated to be less than 1%. A stainless steel distancing ring with low thermal conductivity is placed between the measurement ring and the injector head. For that reason, it is assumed that any axial heat transfer from the cooled segment to the injector head is negligible. In total, the error of the measured heat flow into the cylindrical segment of BKD is estimated to be less than 14% for 700 kW and below 5% for 2000 kW, corresponding to the lower and upper limits of measured heat flows.

D. High-Amplitude Combustion Instability

Two different kinds of high-frequency combustion instabilities have been observed in the BKD test runs. The first type has been investigated in detail by Gröning et al. and is characterized by an excited first transverse (1T) chamber mode with averaged rms amplitudes of about 3.4 bar, which is driven by LOX post eigenmodes [25–27,29]. A second type of instability with higher amplitudes has been described by Armbruster et al. [24]. The raw pressure oscillation

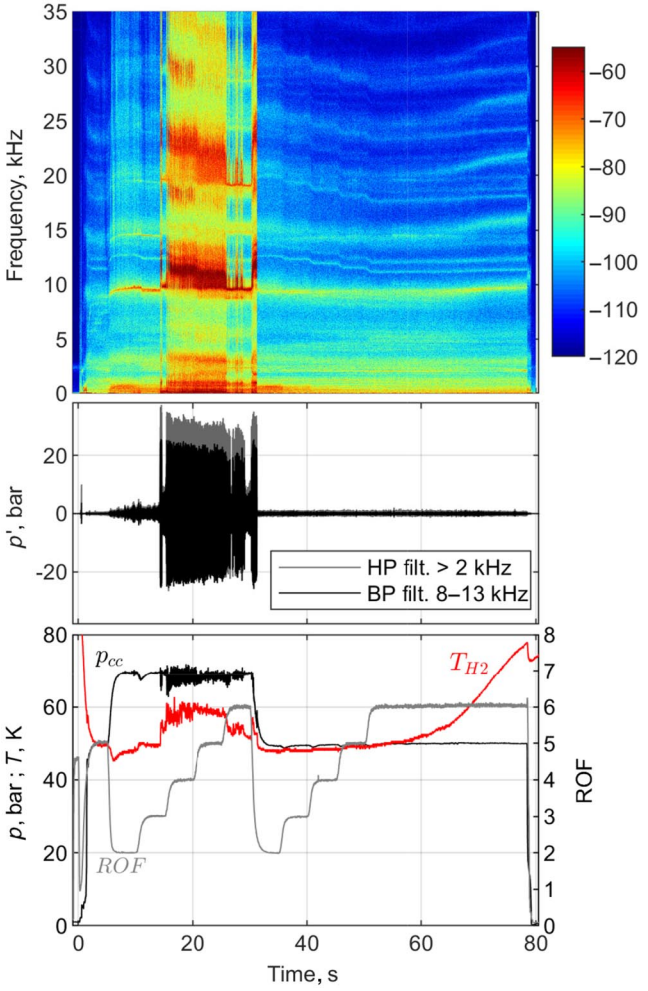

Fig. 3 Test sequence and pressure fluctuation spectrogram of a BKD test run in which the high-amplitude instability occurred from about 14 to 31 s [24].

signal and the corresponding spectrogram for an exemplary test run are presented in Fig. 3. It shows that, in this test run, the high-amplitude combustion instability appears for different operating conditions in the period from about 14–31 s. This instability shows large amplitudes at peak frequencies between 10.4 and 12.1 kHz and occurred in six test runs including different operating conditions. For short periods, the amplitudes even exceeded the sensors' measurement range of ±30 bar. This is equivalent to peak-to-peak values of up to 80% of p_{cc}. Most of the recorded samples are still in the measurement range, and the maximum rms value was 18 bar. The amplitude changes rapidly between periods of low and high amplitudes, while the acoustic-mode shape of the instability resembles that of the 1T chamber mode. The 1T-mode changes from a standing mode for low amplitudes to a fully rotating 1T mode for high amplitudes. Furthermore, the frequency of the oscillation reacts to the amplitude variation and follows with a small time lag. The frequency shifted from a value of about 9.5 kHz for low amplitudes up to almost 12 kHz, an increase of more than 25%. Both observations, the switch from standing to spinning modes as well as the increase in oscillation frequency with growing amplitudes, could be explained by rotating detonationlike traveling waves [6,30,31]. However, the analysis presented by Armbruster et al. showed that, even for the high amplitudes, the oscillation resembles that of an acoustic 1T mode [24]. For this reason, another explanation for the observed frequency shift needs to be present.

A similar effect of shifting eigenmode frequency has also been observed in the research combustor model H (BKH) under acoustic forcing [32,33]. A siren is used to force resonance of the 1T mode of the combustion chamber, and the response of the five clustered

flames was observed via large optical access windows. The frequency increase of the 1T mode during forcing could be explained by observing the impact of transverse acoustic velocity on the flame, which improved mixing and reduced the length of the combustion zone significantly, thereby increasing the speed of sound in the upstream part of the chamber where the 1T mode resides. This behavior in BKH has since been reproduced numerically [22,34]. The effect of tangential acoustic oscillations on flame length in BKD for lower amplitude has also been shown numerically [23,35,36]. The previous experimental investigation of the frequency shift of the 1T mode in BKD for periods of varying transverse pressure amplitudes p' also concluded that the measured frequency shift in BKD could well be explained by a similar flame length reduction mechanism as in BKH [24].

III. Measured Heat Flow

Now that the instability characteristics of BKD are understood, in this paper, the influence of the combustion instability on the experimentally measured heat transfer will be investigated. For most of the test runs, the instability appeared spontaneously and disappeared after a duration on the order of 0.1 s. Due to the thermal inertia of the structure of the combustion chamber, the response time of thermocouples of about 0.2 s, and the time lag of the coolant flow between the inlet and exit thermocouples, the measured heat flow reacts with a delay to changes in the conditions in the chamber. This time lag has been calculated for stable test runs by a cross correlation between changes in operating condition (p_{cc}, ROF) and the responding change in heat flow. The calculated time lag was consistently between 0.3 and 0.4 s. This means that, in most of the test runs, the duration of unstable combustion was not long enough to achieve steady-state heat transfer conditions. Only in two test runs was the high-amplitude combustion instability present for more than 1 s. In one of these runs, the instability appeared during a transient load point change and is therefore challenging to evaluate. Thus, the presented analysis was performed on a single test run with sustained instability and with different operating conditions, which is presented in Fig. 3.

For this work, the heat flow into the cylindrical chamber section is investigated. As mentioned, this integral heat flux in the cylindrical chamber segment $\dot{Q}_{\text{int}}$ is determined using Eq. (1) by means of calculating the change in enthalpy of the water, which is used to cool the chamber walls:

$$\dot{Q}_{\text{int}} = \frac{dH}{dt} = \dot{m} \cdot (h_{\text{out}} - h_{\text{in}}) \tag{1}$$

Here, $\dot{m}$ is the cooling water mass flow rate in the cylindrical segment and h is the specific enthalpy of water. The specific enthalpy values for water were obtained from NIST REFPROP 9.1 using the measured coolant temperature and pressure at the inlet and at the outlet of the chamber.

To quantify increases of heat transfer during unstable combustion, it is necessary to know the heat flow for the same operating condition without instabilities. The well-known, semi-empirical Bartz equation [16] was applied to the BKD conditions but showed large deviation from the measured integral heat flux. These deviations were to be expected, as Bartz is mainly representative for equilibrium conditions, while integral heat fluxes include the entire combustion profile. For that reason, it was decided to use generic correlations to obtain high fit accuracy for the specific BKD data. It was not the goal of this study to find a generally applicable heat flux prediction correlation but rather to determine the increase in heat flow into the cylindrical chamber segment of this experiment during combustion instability. Controlled variables that affect the equilibrium gas properties and thus the heat transfer are ROF, p_{cc}, and the hydrogen injection temperature T_{H_2}. Hence, these were chosen as a basis for a function to fit the heat flow data.

A fully empirical approach was chosen. Optimizing the fit to experimental heat flow data from several different test runs resulted in the fitting function

$$\dot{Q}_{\text{pred}} = a \cdot p_{\text{cc}}^{b_1} \cdot \text{ROF}^{b_2} \cdot T_{H_2}^{b3} + T_{H_2} \cdot b_4 + c \tag{2}$$

The fitting parameters a, b_1, b_2, b_3, b_4, and c are optimized for each test run individually via a least-squares method. This fitting was applied to eight different BKD test data sets. The data sets were preprocessed to remove samples for pressure oscillation amplitudes greater than 5% and during transition between load points so that only stable and steady-state operating conditions are used for the fit.

The obtained fits show mean deviations with respect to the measured data of less than 4% for all test runs and less than 2% for most runs. A comparison of the predicted heat flow by the correlation and the experimentally observed heat flow is shown in Fig. 4 for exemplary test runs with low (Fig. 4a) and high (Fig. 4b) T_{H_2}.

The obtained fits matched the temporal heat flow profiles very closely, which allowed extrapolating throughout the periods of unstable combustion with confidence. During these periods, large deviations to the fitted function were observed. An exemplary analysis is depicted in Fig. 5 (top). Considering the good fit during stable combustion, the deviation can be attributed to increases in heat transfer related to the combustion instabilities.

It is evident in Fig. 5 that the deviation in integral heat flux (Fig. 5 middle) is related to the magnitude of acoustic pressure oscillations (Fig. 5 bottom). During high acoustic amplitudes between 12 and 31 s, a clear increase in integral heat flux of up to 40% is determined, whereas for low amplitudes below 3 bar, there is no clear increase in heat flow. The measured increases of heat flow are significantly larger than the uncertainties in the measured integral heat flow.

However, the increase in the heat flow is surprisingly low for the high amplitudes. This could be due to the fact that other propellant combinations or injector types may lead to a more severe increase in the heat transfer with unstable combustion. Besides, the values of heat transfer increase that are given in literature are significantly larger but are often referring to local heat flux increases in the proximity of the injection plane. BKD has not been equipped with axially distributed cooling circuits. For that reason, an axial heat flux profile and also the distributed heat flux increase cannot be derived from the experiment. However, the measurement ring contains three thermocouples, which reach about 1 mm into hot gas 5.5 mm downstream of the injection plane. In addition, the eight acoustic

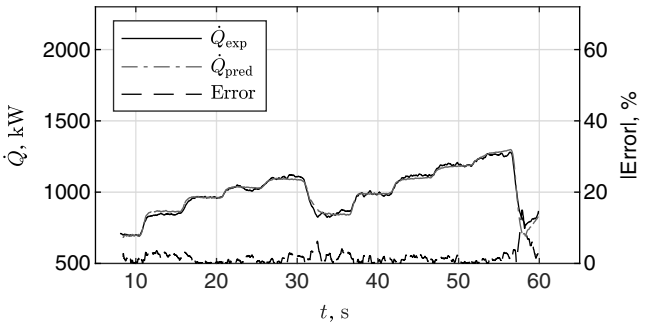

a) Test run with low T_{H_2}

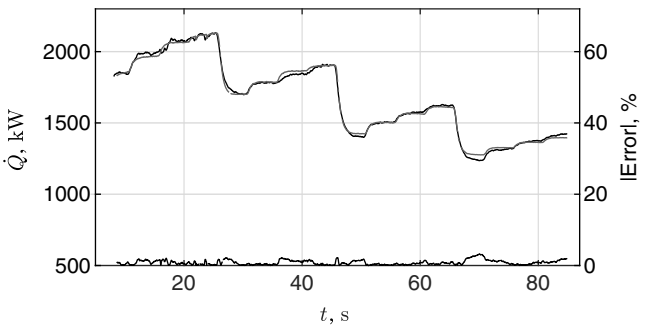

b) Test run with high T_{H_2}

Fig. 4 Fitted heat flow correlation in comparison to experimentally measured heat flow evolution for two exemplary test runs.

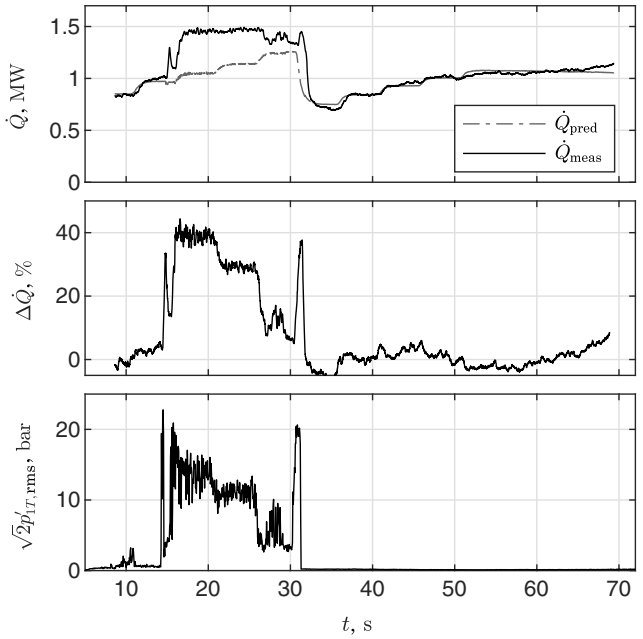

Fig. 5 Comparison of predicted (stable) and measured heat flow during an unstable test.

pressure sensors in the measurement ring are water cooled. The coolant flow is also measured with a turbine flow meter, and the inlet and outlet manifolds of the cooling system contain thermocouples and static pressure sensors. Therefore, the increase in the heat transfer into the sensors, which cover the first 9 mm of the cylindrical chamber, can additionally be investigated. Figure 6 shows the mean hot gas temperature T_{HG} at $x = 5.5$ mm and also the heat flow into the sensor-cooling system $\dot{Q}_{\mathrm{sc}}$ for the unstable test run. The rms amplitudes are also presented.

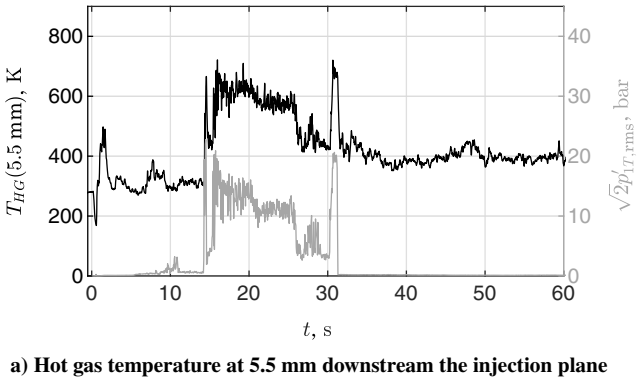

a) Hot gas temperature at 5.5 mm downstream the injection plane

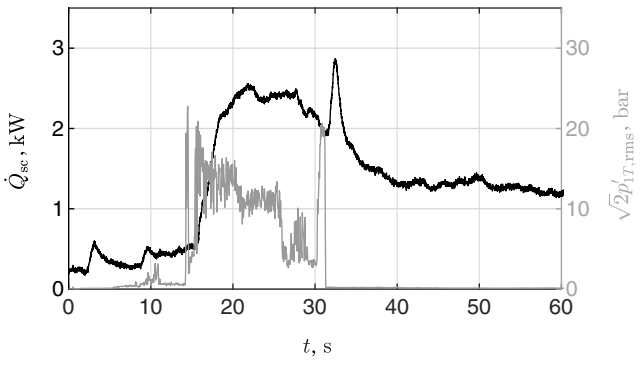

b) Heat flow into the acoustic pressure sensor water cooling

Fig. 6 Thermal loads in the measurement ring for the exemplary test run in Fig. 3.

Both the hot gas temperature in the measurement plane and the heat flow into the sensor cooling show a significant increase during unstable combustion. Due to a slow coolant flow velocity, the sensor-cooling circuit has a delay of a few seconds. However, there is a clear relation of $\dot{Q}_{\mathrm{sc}}$ and the 1T amplitudes with a certain time delay. After the high-amplitude combustion instability appeared, $\dot{Q}_{\mathrm{sc}}$ jumps from 520 W for stable conditions to more than 2200 W and later even to almost 2900 W. After the instability disappeared, the sensor-cooling heat flow drops below 1500 W again. From these values, a localized increase in heat transfer between factors of 1.9 and 5.5 during unstable combustion can be derived. These factors are higher than the integral heat flux into the cylindrical combustion chamber segment and comparable to the values given in literature [1,6]. These observations therefore indicate that the increase in heat flux during unstable combustion is not homogeneously distributed along the chamber axis but seems to have the strongest increase at the head end of the chamber. This is in agreement with heat flux increase observations in a $\mathrm{LOX/CH_4}$ combustion chamber by Hulka and Jones [7].

IV. Model of Heat Flux Distribution

A. Heat Flux Profile

The experiment shows a significant increase in thermal loads during unstable combustion. As was shown, the heat flux increase is not homogeneously distributed but seems to be strongest at the injection plane. In a next step, a theoretical model for heat flux increases due to transverse-mode instabilities will be derived in this paper. This model is based only on the shortening of the combustion zone due to instability and therefore mainly a change in the temperature field. Effects of the acoustic oscillations on the heat transfer coefficient at the chamber wall are neglected. A generic heat flux profile from the injection plane to the end of the chamber cylindrical segment was constructed from three parts: an initial heat flux value at the injector faceplate, an increasing profile corresponding to the length of the flame, and a final value reached for equilibrium burnt gas conditions in the combustion chamber $\dot{q}_{\mathrm{CC}}$. Typical heat flux profiles for multi-element liquid propellant rocket engine combustion chambers can be found in the literature [2,3,37–40]. Experimentally and numerically derived heat flux profiles of comparable combustors were evaluated in order to inform the derivation of a generic profile in BKD and are compared in Fig. 7.

In the example heat flux profiles from literature, it can be observed that the heat flux starts from low initial values at the injection plane and reaches an almost constant heat flux plateau at the end of the cylindrical combustion chamber. The transition from the low initial heat flux to the almost constant value follows approximately an elongated s-shaped increase. The length of this transition correlates with the length of the mixing and combustion zone or, in other words,

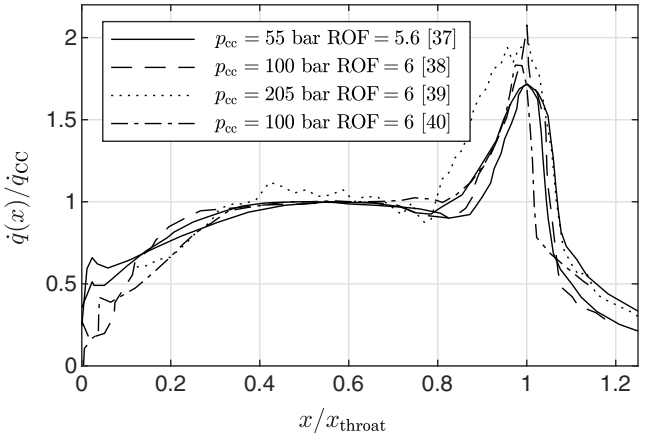

Fig. 7 Exemplary normalized chamber heat flux profiles for supercritical $\mathrm{LOX/H_2}$ combustion adjusted from published profiles [37–40].

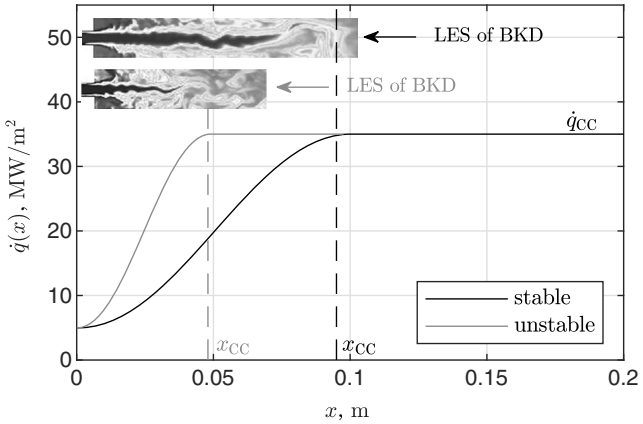

Fig. 8 Generic BKD heat flux profiles illustrating the impact of the shortened combustion zone due to transverse combustion instability. The overlaid images of flames for stable and unstable conditions of BKD have been adjusted from LES results of Schmitt et al. [35].

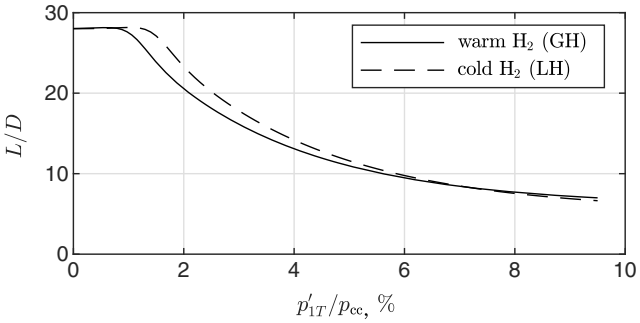

Fig. 9 Correlation of LOX core length reduction as a function of relative transverse-mode amplitude for different operating conditions in a rectangular chamber (curves adjusted from [20,42]).

the flame length. After the combustion is completed, the mean flowfield does not show large variation in the axial direction, which explains the constant plateau of $\dot{q}$ at the downstream end of the cylindrical combustion chamber.

For the experimental combustion chamber BKD, a detailed heat flux profile does not exist. However, a simplified profile based on the published profiles in Fig. 7 can be derived. The initial heat flux value at the injector face is assumed to depend mostly on the temperatures of the injected propellants. Experimental results of combustors with comparable operating conditions are between 0 and 10 MW/m^2, with dependence on hydrogen inlet temperatures [38,41]. The value reached after completed combustion $\dot{q}_{CC}$ could be estimated using the Bartz equation and has an average value of around 35 MW/m^2 for the range of operating conditions in BKD. This value is consistent with those in the examples displayed in Fig. 7, which range from about 31 MW/m^2 for $p_{cc} = 55$ bar and ROF = 5.6 [37] to 45 MW/m^2 for $p_{cc} = 100$ bar and ROF = 6 [3,38,39].

Figure 8 shows the resulting, generic heat flux profile that is assumed for BKD in this study. The transition from the initial lower heat flux value to the almost constant plateau is hereby described by part of a sine function (from $-\pi/2$ to $\pi/2$). As described before, the length of that s-shaped increase is thereby depending on the length of the combustion zone x_{CC}. Two flame solutions from large eddy simulation (LES) results of BKD [35] for stable and unstable conditions are also presented. Based on the shorter flame for unstable conditions, chemical equilibrium and thus the constant $\dot{q}$ plateau is achieved earlier in the combustion chamber.

From the two simplified heat flux profiles in Fig. 8, it can already be observed that the shorter flames will lead to a local $\dot{q}(x)$ increase in the first part of the chamber and also to an increase in the integral heat flux in the cylindrical combustion chamber. However, in order to quantify this flame-shortening effect on the local and integral heat transfer, an expression for the flame length as a function of the transverse acoustic oscillations is required. This flame retraction submodel will be described in the next paragraph.

B. Flame Retraction Submodel

To construct an experimental model that can predict the observed increases in heat flow due to the flame-shortening process, observations from the aforementioned BKH were used as a basis. While a siren incorporated in the upper wall subjects the five central flames to a high-amplitude, transverse acoustic field, backlit shadowgraph imaging reveals how the LOX core decreases in length due to accelerated breakup and mixing driven by the transverse acoustic velocity oscillations. By virtue of the high frame rate of the imaging, the length of the intact part of the LOX core could be measured with dependence on the acoustic amplitude [20,21]. Cases from BKH were selected based on their similarity to operating conditions in BKD, namely supercritical pressure and both high and low T_{H_2}, and the similarity in injector geometry between BKH and BKD. Examples of fitted LOX core length profiles are shown in Fig. 9.

The fit expressions are

$$\frac{L}{D_{BKH}} = 29.55 \cdot 0.7^{p'_{\%}} + 6 \tag{3}$$

and

$$\frac{L}{D_{BKH}} = 34.97 \cdot 0.71^{p'_{\%}} + 5.29 \tag{4}$$

for high and low T_{H_2} cases, respectively. While measurements in BKH did not extend beyond a relative amplitude of 9.7%, the asymptotic behavior is assumed to result in minimal error for extrapolation to the higher amplitude reached in BKD. Note that the flame shortening is driven by its interaction with the transverse acoustic velocities u' rather than the pressure amplitudes directly. However, because transverse velocities cannot be measured with the given setup, the flame retraction correlations are given as a function of measured relative pressure amplitudes at the chamber wall.

For this reason, although normalized, these expressions are not generalized. For example, a transverse pressure wave in the rectangular geometry of BKH with centrally clustered injectors will not induce the same transverse velocities over the injector as a tangential-mode wave of the same amplitude in a chamber with cylindrical geometry, such as BKD. To generalize Eq. (5), the pressure amplitudes shall be scaled to compensate for the difference in induced acoustic velocities, as shown in Eq. (6), where the effective velocity u'_{eff} is the mean transverse velocity magnitude at the position of a given LOX jet. Equations (3) and (4) were scaled by relative transverse acoustic velocities according to

$$\frac{L}{D_{BKH}} = f(p'_{\%}) \tag{5}$$

$$\frac{L}{D_{BKD}} = f\left(p'_{\%} \cdot \frac{u'_{BKD_{eff}}}{u'_{BKH_{eff}}}\right) \tag{6}$$

For BKH, this is relatively simple to calculate due to the rectangular, high-aspect-ratio geometry of the combustion chamber and central location of the injector elements. This allows the velocity to be estimated as a function of acoustic pressure amplitudes p' with the one-dimensional standing wave formula. Thus, the effective velocity averaged over one cycle in this case is

$$u'_{BKH_{eff}} = \frac{1}{\rho \cdot u_c}\hat{p}' \cdot \frac{1}{\sqrt{2}} \tag{7}$$

where $\hat{p}'$ is the 1T amplitude measured at the wall, and ρ and u_c are the mean density and speed of sound of the combustion gases in the chamber, respectively. Example calculations for different ROF values and chamber pressures are shown in Fig. 10 [20,34,42].

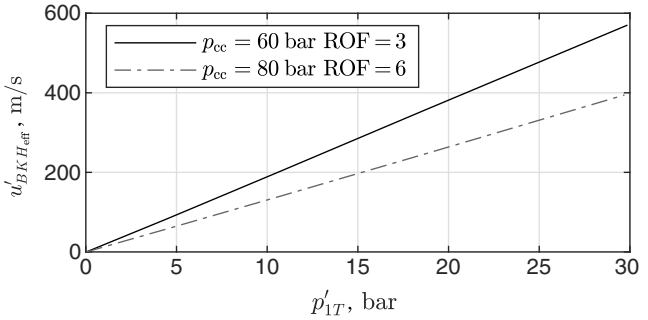

Fig. 10 Estimated mean transverse velocities at the injector in the BKH combustor.

Estimating u'_{eff} in BKD is not so straightforward because the circular chamber cross section and rotational character of the 1T mode need to be taken into account. To describe the rotational character, experimental data were available from seven of the eight acoustic pressure sensors that were flush mounted near the injector plate and equally spaced around the circumference. Figure 11 shows the p' signals, bandpass filtered around the 1T mode, describing a standing 1T mode for low p' amplitude (Fig. 11a) and a fully rotating mode for higher amplitude (Fig. 11b). Standing wave behavior was consistently observed for amplitudes below 10 bar, and a rotating mode was consistently observed for amplitudes above 15 bar [24].

The analytic solution for the pressure distribution of the first tangential eigenmode of a cylindrical volume was taken from Sliphorst et al. for standing and spinning modes [43]. The corresponding velocity field can be obtained from Euler's equation as

$$u'(\theta, r_\theta, t) = -\frac{1}{\rho}\int \nabla p'(\theta, r_\theta, t)\,\mathrm{d}t \tag{8}$$

where $\nabla p'(\theta, r_\theta)$ is the gradient of the 1T pressure field in polar coordinates and ρ the mean density in the chamber taken at combustion equilibrium, just as for BKH. The resulting pressure and velocity fields for standing and rotating 1T modes are given in Fig. 12. The velocity field has a 90 deg phase offset with respect to the pressure field.

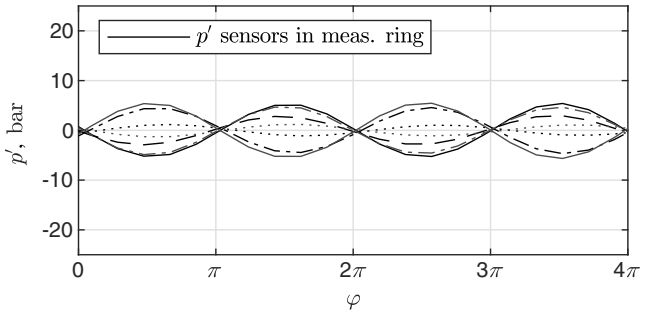

a) Standing 1T mode for moderate amplitudes

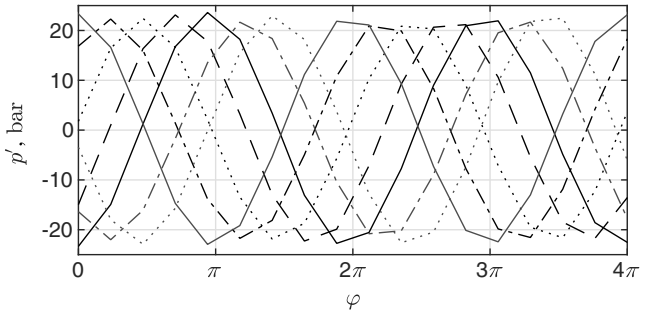

b) Spinning 1T mode for high amplitudes

Fig. 11 Chamber 1T-mode characteristics for the exemplary test run in Fig. 3.

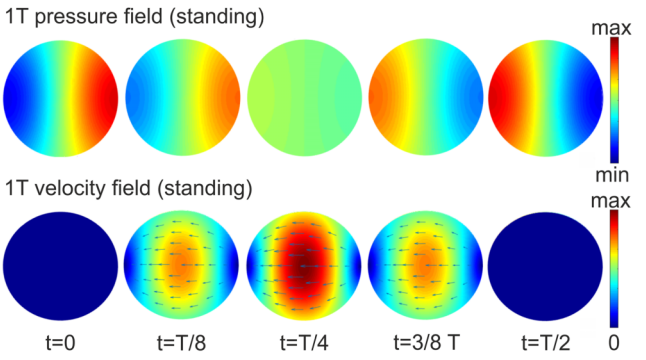

a) Standing 1T

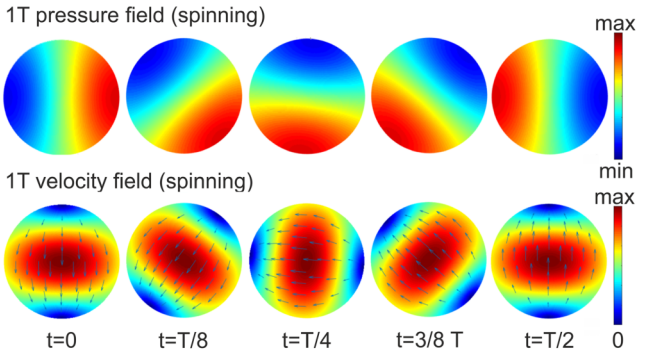

b) Spinning 1T

Fig. 12 1T-mode pressure and velocity field distributions at the injection plane in BKD.

Having defined the transverse velocity fields, the magnitude as projected onto the injector locations can be determined. In this work, only the outer ring of injector elements is considered. The flames of these injectors are adjacent the chamber wall and therefore dominate the contribution of heat flux into the walls. Transverse velocities near the wall are the lowest, and so the flames are expected to retract the least, thus acting as a boundary between shorter, inner-row injector flames. To relate local transverse velocities to p' at the wall in BKD, a standing wave is assumed for amplitudes below 10 bar and rotating waves above 10 bar. Resulting local transverse velocities are plotted in Fig. 13 for the three rows of elements.

Although not the focus of this study, this estimate of effective convective velocities at the chamber walls does allow the possibility for an enhanced heat transfer coefficient to be evaluated. Both axial and transverse velocities can be estimated by making use of the axial speed of sound and Mach number profiles in BKD calculated by Schulze and Sattelmayer [44,45]. Acoustic velocities were estimated by scaling the acoustic velocity magnitude as calculated for

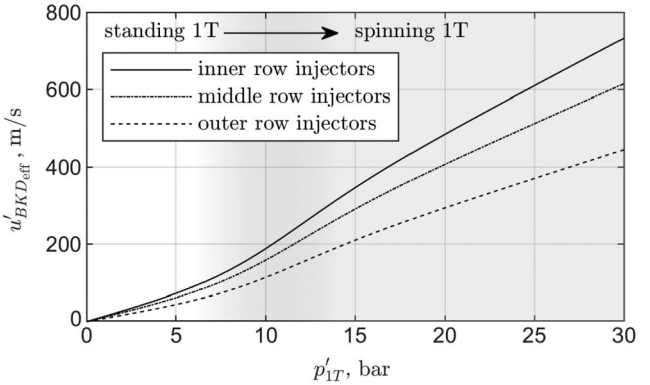

Fig. 13 Transverse acoustic velocity local to injectors arranged in three rows as a function of acoustic pressure amplitude measured at the wall in BKD.

Table 1 Estimated increases in convective velocities

x, m	u_c, m/s	M	Axial velocity, m/s	u', m/s	Scaling factor	u'_{real}, m/s	Total velocity, m	Factor increase
0	1100	0.060	66	259	1.00	259	267	4.1
0.025	1400	0.075	105	329	0.75	263	283	2.6
0.05	1450	0.100	145	341	0.50	188	237	1.4
0.1	1700	0.225	383	400	0.25	100	396	1.0
0.2	1700	0.225	383	400	0.05	20	384	1.0

completed combustion in Fig. 13 with the respective speed of sound at each chamber section. As transverse pressure amplitude decays toward the end of the chamber, the acoustic velocities were scaled with the axial 1T-mode amplitude profile from Schulze and Sattelmayer [44,45], and finally a comparison can be made between acoustic velocities and mean flow velocities. From results presented in Table 1, a maximum convective velocity increase over the combustor walls of a factor of 4 can be found at the injector faceplate, a factor of 2.6 immediately after injection, and no increase following completion of combustion. From Bartz, the heat flux is proportional to the convective velocity to the power 0.8, meaning a heat transfer increase of a factor of 3 can be expected at the injector faceplate, which follows the same trend as the convective velocity by dropping quickly to a factor of 2.2 and disappearing as pressure amplitudes dampen out. In the case of BKD, this increase only applies to a very small region directly at the injector faceplate. In conclusion, the local increases in convective velocities is thought to be a significant contributor that should be better quantified, although this effect alone is insufficient to explain the reported factors of 4–10 increases in heat transfer in literature [1,5,6]. Further analysis is outside the scope of the study presented in this paper.

Instead, an explanation for the remaining gap in heat transfer increase will be offered, showing that the flame length reduction can explain both the lower heat flow increase in the experiment (up to 40%) as well as high local increases in heat flux of up to 1000%.

The absolute intact LOX jet length of the outer row of injectors, estimated from Eq. (6), is shown in Fig. 14. The model output is referred to as flame length because the intact LOX jet length strongly defines the topology of the reaction zone of a flame and therefore the heat flux experienced by a neighboring wall surface. Further verification of this estimated flame length was sought from CFD results. BKD has become a well-known test case for numerical modeling of combustion instabilities [23,35,36,45,46]. There have been several CFD simulations of BKD for different operating conditions and acoustic amplitudes. All of the simulations show flame shortening and can therefore be compared with the flame length model for BKD, shown as points overlaid in Fig. 14. From the CFD solutions [23,35,36], the flame lengths were visually estimated for stable and unstable conditions. In all simulations, a reduction in flame length was observed for transverse oscillations. Despite high uncertainty in measuring the flame length from the CFD solutions, and excepting one outlier, the trend of flame length reduction from the simulations is well reproduced by the derived model.

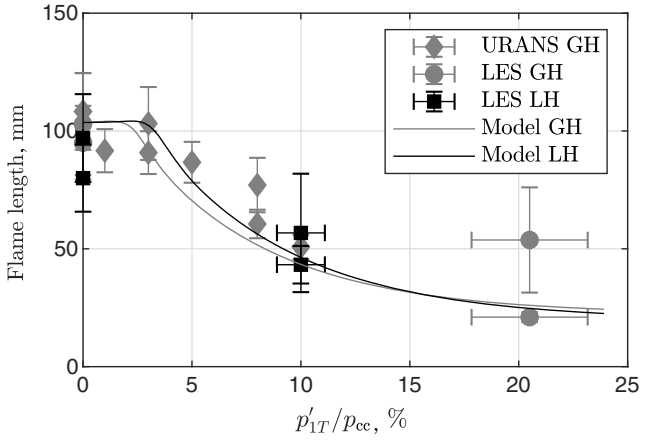

Fig. 14 Comparison of the applied BKD flame length model with BKD simulation results: URANS GH [23], LES GH [36], LES LH [35].

V. Results and Discussion

The flame length correlation derived in the paper before was used to estimate heat flux profiles for the range of unstable amplitudes observed in BKD. Due to the flame-shortening process, the length of the combustion zone decreases, and chemical equilibrium is achieved earlier in the chamber. For that reason, the location where the $\dot{q}(x)$ profile plateaus moves upstream, as shown in Fig. 15 for varying 1T amplitudes. As was described before, the model is based only on the flame-shortening process. This explains why the strongest $\dot{q}$ increase appears at the head end of the chamber, whereas there is no increase at the downstream end. In a LOX/CH_4 research combustor, the greatest increase in heat flux was observed close to the faceplate [7], which is consistent with the model here. However, in that experiment there was also a significant increase in heat flux at the downstream end of the cylindrical chamber section. This effect cannot be captured by the derived model because any influence of the instability on the heat transfer coefficient is neglected.

In this section, the model will be compared to the measurements from BKD to understand the extent to which changes in flame length can explain experimental observations from combustion instability events.

A. Comparison with Experiment

There are no axially resolved measurements of heat flux distribution in BKD available to date, and so the results of the model were compared to the integrated value from the cylindrical segment in the experiment. The axial heat flux profiles were integrated over the length of the cylindrical combustion chamber segment. The resulting heat flow for varying amplitudes was normalized by the stable heat flow in order to calculate relative increases of heat transfer as a function of instability amplitudes. The resulting changes in heat flow with varying amplitudes of acoustic pressures are shown in Fig. 16. As was described before, in the model, a standing mode is assumed for amplitudes below 10 bar and a fully spinning mode for amplitudes higher than 10 bar. This assumption is based on experimental observations of the acoustic field dynamics [24]. For a spinning 1T mode, the acoustic velocity reaches a higher effective value over one cycle than for a standing 1T mode. Therefore, the modeled normalized heat flow increase shows a discontinuity at 10 bar. A smoothed model curve is also presented in the Fig. 16. After the transition from

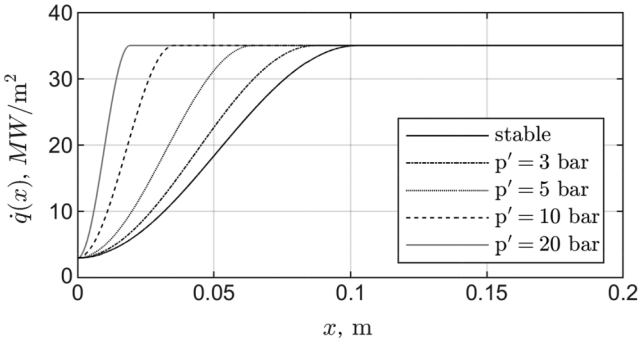

Fig. 15 Predicted axial heat flux profiles in the cylindrical combustion chamber segment for different transverse-mode instability amplitudes.

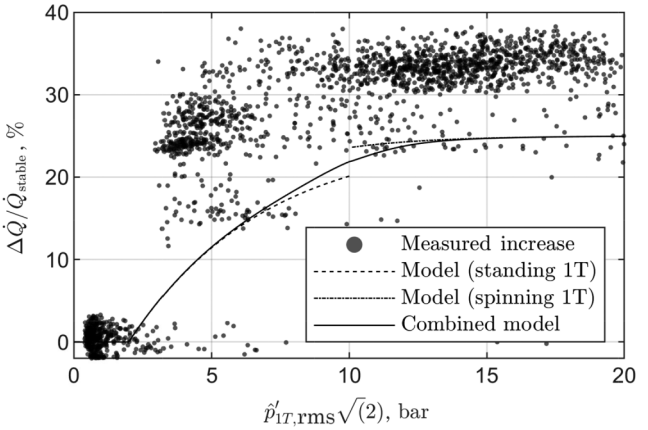

Fig. 16 Comparison of predicted with experimental increase in integral heat flux.

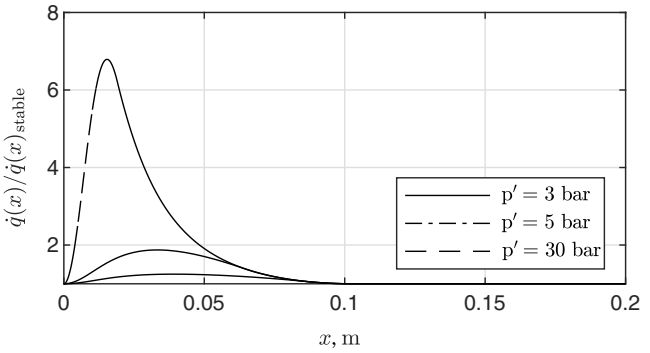

Fig. 17 Predicted local heat flux for different instability amplitudes.

standing to a fully spinning 1T mode, the heat flow increase approaches an asymptotic value in the model because the flame length reaches a minimum, as can be seen in Fig. 9. A similar asymptotic limit of the heat transfer rate increase can be observed in the experimental results. In the experiment, there seems to be a sudden $\Delta\dot{Q}$ increase at an amplitude of about 3 bar. This can partially be explained by the flame length observations from BKH (see Fig. 9). There seems to be a certain threshold for the flame length reduction. If the amplitudes stay below that threshold, the flame length is not significantly affected by the acoustic perturbation.

The relative increase in integral heat flux predicted by the model is in a similar range as the experiment. It shows almost no effect on heat flow for low amplitudes, whereas for larger amplitudes, the model predicts increases of up to 25%, depending on the operating conditions, the initial heat flux value at $x = 0$, and the flame length for stable combustion. This is less than the experimentally measured increase (30–40%) but still in a similar range.

The comparison between the model and the heat flow measurements in Fig. 16 shows that the published flame-shortening relationship of BKH can be modified for cylindrical combustion chambers and combined with a generic heat flux profile. The comparison also demonstrates that, under the given assumptions, the model is able to predict both the trend and a large fraction of the experimental heat flow increase. This observation therefore suggests that, in BKD, the majority of the heat transfer increase during unstable combustion could be driven by a significant shortening of the combustion zone.

However, the remaining 3–18% deviation in relative heat flow increase between experiment and model highlights that other processes are likely to contribute to the change in local heat flux. This includes most probably a destruction of the thermal boundary layer and an increase in convective heat transfer due to induced transverse flows over the combustor walls, among others. Accounting for these effects is outside the scope of the current work.

B. Local Increases in Heat Flux

The measured and predicted increases of integral heat transfer in BKD are low regarding the high amplitudes of the combustion instability. However, it has to be noted that the aforementioned large increases of heat fluxes given in literature of factors 4–12 are often referring to increases in the local heat flux close to the injection plane, where thermal damage is typically observed. The investigation of the heat flow into the sensor-cooling circuit expanding the first 10 mm of the combustion chamber also demonstrated that increases in local heat flux at the head end of the chamber are significantly larger than the integrated heat flow increase. Therefore, it is analyzed if the model is able to predict the local increases in heat flux with respect to the stable heat flux profile. Figure 17 shows the axial distribution of heat flux increases for amplitudes of 3, 5, and 30 bar. Low amplitudes have little impact on the local heat flux, which may not directly lead to thermal damage of the chamber walls. However, for a relatively modest amplitude of 5 bar, the local heat flux can almost double in the first half of the chamber. For 30 bar amplitude, the model predicts a local increase of almost a factor of 7, which is more in agreement with the levels reported in literature and the observed experimental increases of the thermal loads in the BKD measurement ring.

The local increases of multiples of the stable heat flux can lead to thermal damage of regeneratively cooled flight engines, with a low margin on the maximum chamber wall temperature. The location of the peak increase in thermal load predicted by the model is close to the injection plane and therefore also in agreement with many reported failures of LPREs due to high-frequency combustion instabilities.

VI. Conclusions

In this study, the increase in the wall heat transfer due to transverse-mode high-frequency combustion instabilities in a 42-element LOX/H_2 rocket combustion chamber was investigated. The combustion instabilities are of the 1T-mode type, and the amplitudes exceed 80% of the mean chamber pressure. The analysis of the water-cooling circuit of the cylindrical combustion chamber showed that the integral heat flow increases by up to 40%. Thermocouples and a sensor-cooling circuit in the measurement plane 5.5 mm downstream of the injection plane in BKD indicate a much higher increase in the local heat flux of more than 4.4-fold. Therefore the heat flux increase is not homogeneously distributed in the chamber but seems to be strongest in the injection region.

A new model for predicting local increases in heat flux due to transverse combustion instabilities was derived. The model is based on the change in flame length, which is caused by transverse acoustic oscillations. The relation for flame length dependency on acoustic amplitude was generalized for use in a cylindrical combustion chamber from past experimental measurements performed in a rectangular combustor. The integrated heat flux from the predicted heat flux profile was compared with the integral heat flux increases measured in the experiment. Predicted increases in heat flow are around 25% for high amplitudes and different conditions. The model also predicts local increases in heat flux near the injector face, which are much larger than the integrated heat flux, reaching up to a factor of 7 with respect to stable combustion. This agrees well with cases reported in literature and can explain cases of molten injector plates where the rest of the combustion chamber seemed unaffected after combustion instabilities.

However, the change in temperature distribution described by the model does not account for the 40% increase in measured integral heat flow. Therefore, this study also indicated that other effects, such as thermal boundary layer disruption or increases in convective velocities, could be responsible for the remaining heat flow increase.

The results of this study suggest that flame length reduction during transverse-mode combustion instabilities is the dominant process contributing to heat flux increases close to the faceplate, which can lead to critical failures in industrial flight engines While the model was developed for an LOX/H_2 experimental combustor with shear coaxial injectors, the principles on which it is based should be applicable to other liquid propellant rocket engines. Nevertheless, future studies are required to investigate how the flame shortening

affects the heat flux increase during unstable combustion for other experimental conditions, such as varying propellant types, injectors, and acoustic-mode shapes.

To the authors' knowledge, the present study presents the first model that is able to explain the damaging increase in heat flux due to high-frequency combustion instabilities. Current limitations of the described model are a restriction to transverse modes and neglecting the influence of acoustic oscillations on the heat transfer coefficient. Effects on the heat transfer coefficient should be added in future studies in order to obtain a more generalized prediction of heat flux increase due to high-frequency combustion instabilities.

Acknowledgments

Financial support has been provided by the German Research Foundation (Deutsche Forschungsgemeinschaft, DFG) in the framework of the Sonderforschungsbereich Transregio 40 (SFB-TRR40). The work is also associated with the Franco-German Rocket Engine Stability iniTiative (REST). The authors would like to thank the crew of the P8 test bench for their support in running the BKD hot-fire tests on which the results presented here are based.

References

[1] Sutton, G. P., and Biblarz, O., *Rocket Propulsion Elements*, 8th ed., Wiley, New York, 2010, Chap. 9.3.

[2] Huang, D., and Huzel, D., *Modern Engineering for Design of Liquid-Propellant Rocket Engines*, edited by R. Seebas, Vol. 147, Progress in Astronautics and Aeronautics, AIAA, Reston, VA, 1992, Chaps. 4.4, 4.8. https://doi.org/10.2514/4.866197

[3] Schmidt, G. (ed.), *Technik der Flüssigkeits-Raketentriebwerke*, DaimlerChryslerAerospace, Taufkirchen, Germany, 1999, Chap. 4.4.5.

[4] Yang, V., and Anderson, W. (eds.), *Liquid Rocket Engine Combustion Instability*, AIAA, Washington, D.C., 1995.

[5] Dranovsky, M. L. (ed.), *Combustion Instabilities in Liquid Rocket Engines: Testing and Development Practices in Russia*, Progress in Astronautics and Aeronautics, AIAA, Reston, VA, 2007, pp. 43–44. https://doi.org/10.2514/4.866906

[6] Harrje, D., and Reardon, F., (eds.), "Liquid Propellant Rocket Combustion Instability," NASA SP-194, 1972.

[7] Hulka, J., and Jones, G., "Performance and Stability Analyses of Rocket Combustion Devices Using Liquid Oxygen/Liquid Methane Propellants," AIAA Paper 2010-6799, 2010. https://doi.org/10.2514/6.2010-6799

[8] Deeken, J., Suslov, D., Schlechtriem, S., and Haidn, O., "Impact of Injection Distribution on Cryogenic Rocket Engine Stability," *Progress in Propulsion Physics*, Vol. 4, March 2013, pp. 149–166. https://doi.org/10.1051/eucass/201304149

[9] Rubinsky, V. R., "Combustion Instability in the RD-0110 Engine," *Liquid Rocket Engine Combustion Instability*, edited by V. Yang, and W. E. Anderson, AIAA, Washington, D.C., 1995, pp. 89–112, Chap. 4.

[10] Fisher, S. C., Dodd, F. E., and Jensen, R. J., "Scaling Techniques for Liquid Rocket Combustion Stability Testing," *Liquid Rocket Engine Combustion Instability*, edited by V. Yang, and W. E. Anderson, AIAA, Washington, D.C., 1995, pp. 545–564, Chap. 21.

[11] Conrad, E., Bloomer, H. E., Wanhainen, J. P., and Vincent, D. W., "Interim Summary of Liquid Rocket Acoustic-Mode-Instability Studies at a Nominal Thrust of 20000 Pounds," NASA Lewis Research Center, NASA TN D-4968, Cleveland, OH, 1968.

[12] Laudien, E., Pongratz, R., Pierro, R., and Preclik, D., "Experimental Procedures Aiding the Design of Acoustic Cavities," *Liquid Rocket Engine Combustion Instability*, edited by V. Yang, and W. E. Anderson, AIAA, Washington, D.C., 1995, pp. 377–399, Chap. 14.

[13] Dec, J. E., and Keller, J. O., "Pulse Combustor Tail-Pipe Heat-Transfer Dependence on Frequency, Amplitude, and Mean Flow Rate," *Combustion and Flame*, Vol. 77, Nos. 3–4, 1989, pp. 359–374. https://doi.org/10.1016/0010-2180(89)90141-7

[14] Dec, J. E., Keller, J. O., and Arpaci, V. S., "Heat Transfer Enhancement in the Oscillating Turbulent Flow of a Pulse Combustor Tail Pipe," *International Journal of Heat and Mass Transfer*, Vol. 35, No. 9, 1992, pp. 2311–2325. https://doi.org/10.1016/0017-9310(92)90074-3

[15] van Buren, S., and Polifke, W., "Heat Transfer in Pulsating Flow and Its Impact on Temperature Distribution and Damping Performance of Acoustic Resonators," *Future Space-Transport-System Components Under High Thermal and Mechanical Loads: Results from the DFG Collaborative Research Center TRR40*, edited by N. A. Adams, W. Schröder, R. Radespiel, O. J. Haidn, T. Sattelmayer, C. Stemmer, and B. Weigand, Springer International Publishing, Cham, Switzerland, 2021, pp. 97–111. https://doi.org/10.1007/978-3-030-53847-7_6

[16] Bartz, D., "A Simple Equation for Rapid Estimation of Rocket Nozzle Convective Heat Transfer Coefficients," *Journal of Jet Propulsion*, Vol. 27, June 1957, pp. 49–53. https://doi.org/10.2514/8.12572

[17] Hakim, L., Ruiz, A., Schmitt, T., Boileau, M., Staffelbach, G., Ducruix, S., Cuenot, B., and Candel, S., "Large Eddy Simulations of Multiple Transcritical Coaxial Flames Submitted to a High-Frequency Transverse Acoustic Modulation," *Proceedings of the Combustion Institute*, Vol. 35, No. 2, 2015, pp. 1461–1468. https://doi.org/10.1016/j.proci.2014.05.142

[18] Hakim, L., Schmitt, T., Ducruix, S., and Candel, S., "Dynamics of a Transcritical Coaxial Flame Under a High-Frequency Transverse Acoustic Forcing: Influence of the Modulation Frequency on the Flame Response," *Combustion and Flame*, Vol. 162, No. 10, 2015, pp. 3482–3502. https://doi.org/10.1016/j.combustflame.2015.05.022

[19] Hardi, J. S., Beinke, S. K., Oschwald, M., and Dally, B. B., "Coupling of Cryogenic Oxygen-Hydrogen Flames to Longitudinal and Transverse Acoustic Instabilities," *Journal of Propulsion and Power*, Vol. 30, No. 4, 2014, pp. 991–1004. https://doi.org/10.2514/1.B35003

[20] Hardi, J. S., Martinez, C. G. H., Oschwald, M., and Dally, B. B., "LOx Jet Atomization Under Transverse Acoustic Oscillations," *Journal of Propulsion and Power*, Vol. 30, No. 2, 2014, pp. 337–349. https://doi.org/10.2514/1.B34979

[21] Hardi, J., and Oschwald, M., "Cryogenic Oxygen Jet Response to Transverse Acoustic Excitation with the First Transverse and the First Combined Longitudinal-Transverse Modes," *Progress in Propulsion Physics*, Vol. 8, July 2016, pp. 75–94. https://doi.org/10.1051/eucass/201608075

[22] Beinke, S. K., Hardi, J. S., Banuti, D. T., Karl, S., Dally, B. B., and Oschwald, M., "Experimental and Numerical Study of Transcritical Oxygen-Hydrogen Rocket Flame Response to Transverse Acoustic Excitation," *Proceedings of the Combustion Institute*, Vol. 38, No. 4, 2020, pp. 5979–5986. https://doi.org/10.1016/j.proci.2020.05.027

[23] Schulze, M., and Sattelmayer, T., "Flame Dynamics in Supercritical H2/O2 Rocket Combustion Systems," *Annual Report*, edited by N. Adams, R. Radespiel, T. Sattelmayer, W. Schroeder, and B. Weigand, Sonderforschungsbereich/Transregio 40, 2015.

[24] Armbruster, W., Hardi, J. S., Suslov, D., and Oschwald, M., "Experimental Investigation of Self-Excited Combustion Instabilities with Injection Coupling in a Cryogenic Rocket Combustor," *Acta Astronautica*, Vol. 151, Oct. 2018, pp. 655–667. https://doi.org/10.1016/j.actaastro.2018.06.057

[25] Gröning, S., Hardi, J. S., Suslov, D., and Oschwald, M., "Injector-Driven Combustion Instabilities in a Hydrogen/Oxygen Rocket Combustor," *Journal of Propulsion and Power*, Vol. 32, No. 3, 2016, pp. 560–573. https://doi.org/10.2514/1.B35768

[26] Gröning, S., Hardi, J. S., Suslov, D., and Oschwald, M., "Influence of Hydrogen Temperature on the Stability of a Rocket Engine Combustor Operated with Hydrogen and Oxygen," *CEAS Space Journal*, Vol. 9, No. 1, 2017, pp. 59–76. https://doi.org/10.1007/s12567-016-0130-8

[27] Gröning, S., Hardi, J., Suslov, D., and Oschwald, M., "Measuring the Phase Between Fluctuating Pressure and Flame Radiation Intensity in a Cylindrical Combustion Chamber," *Progress in Propulsion Physics*, Vol. 11, Feb. 2019, pp. 425–446. https://doi.org/10.1051/eucass/201911425

[28] Haemisch, J., Suslov, D., and Oschwald, M., "Experimental Study of Methane Heat Transfer Deterioration in a Subscale Combustion Chamber," *Journal of Propulsion and Power*, Vol. 35, No. 4, 2019, pp. 819–826. https://doi.org/10.2514/1.B37394

[29] Armbruster, W., Hardi, J. S., Suslov, D., and Oschwald, M., "Injector-Driven Flame Dynamics in a High-Pressure Multi-Element Oxygen-Hydrogen Rocket Thrust Chamber," *Journal of Propulsion and Power*, Vol. 35, No. 3, 2019, pp. 632–644. https://doi.org/10.2514/1.B37406

[30] Clayton, R. M., Rogero, R. S., and Sotter, J. G., "An Experimental Description of Destructive Liquid Rocket Resonant Combustion," *AIAA Journal*, Vol. 6, No. 7, 1968, pp. 1252–1259. https://doi.org/10.2514/3.4730

[31] Ar'kov, O. F., Voitsekhovskii, B. V., Mtrofanoc, V. V., and Topchiyan, M. E., "On the Spinning-Detonation-Like Properties of High Frequency Tangential Oscillations in Combustion Chambers of Liquid Fuel Rocket Engines," *Zhurnal Prikadnoi Mekhaniki i Tekhnicheskoi Fiziki*, Vol. 11, No. 1, 1970, pp. 155–157, https://link.springer.com/content/pdf/10.1007/BF01102693.pdf.

[32] Kawashima, H., Hardi, J., Webster, S., and Oschwald, M., "Combustor Resonance Frequency Under Unstable Combustion," *30th International Symposium on Space Technology and Science (ISTS) 2015*, JSASS Paper 2015-a58, 2015.

[33] Webster, S., Hardi, J., and Oschwald, M., "One-Dimensional Model Describing Eigenmode Frequency Shift During Transverse Excitation," *Progress in Propulsion Physics*, Vol. 11, Feb. 2019, pp. 273–294. https://doi.org/10.1051/eucass/201911273

[34] Hardi, J. S., Traudt, T., Bombardieri, C., Börner, M., Beinke, S. K., Armbruster, W., Blanco, P. N., Tonti, F., Suslov, D., Dally, B., and Oschwald, M., "Combustion Dynamics in Cryogenic Rocket Engines: Research Programme at DLR Lampoldshausen," *Acta Astronautica*, Vol. 147, Feb. 2018, pp. 251–258. https://doi.org/10.1016/j.actaastro.2018.04.002

[35] Schmitt, T., Staffelbach, G., Ducruic, S., Gröning, S., Hardi, J., and Oschwald, M., "Large-Eddy Simulations of a Sub-Scale Liquid Rocket Combustor: Influence of Fuel Injection Temperature on Thermo-Acoustic Stability," *7th European Conference for Aeronautics and Aerospace Sciences (EUCASS) 2017*, EUCASS Paper 2017-352, 2017. https://doi.org/10.13009/EUCASS2017-352

[36] Urbano, A., Selle, L., Staffelbach, G., Cuenot, B., Schmitt, T., Ducruix, S., and Candel, S., "Exploration of Combustion Instability Triggering Using Large Eddy Simulation of a Multiple Injector Liquid Rocket Engine," *Combustion and Flame*, Vol. 169, July 2016, pp. 129–140. https://doi.org/10.1016/j.combustflame.2016.03.020

[37] Eiringhaus, D., Riedmann, H., Knab, O., and Haidn, O. J., "Full-Scale Virtual Thrust Chamber Demonstrators as Numerical Testbeds Within SFB-TRR40," AIAA Paper 2018-4469, 2018.

[38] Masquelet, M. M., "Simulations of a Sub-Scale Liquid Rocket Engine: Transient Heat Transfer in a Real Gas Environment," Ph.D. Thesis, Georgia Inst. of Technology, Atlanta, GA, 2006.

[39] Dexter, C. E., Fisher, M. F., Hulka, J. R., Denisov, K. P., Shibanov, A. A., and Agarkov, A. F., "Scaling Techniques for Design, Development, and Test," *Liquid Rocket Thrust Chambers: Aspects of Modeling, Analysis, and Design*, AIAA, Reston, VA, 2004, pp. 553–600, Chap. 16. https://doi.org/10.2514/5.9781600866760.0553.0600

[40] Ivancic, B., Riedmann, H., and Frey, M., "Validation of Turbulent Combustion Models for 3D-Simulations of Liquid H2/O2 Rocket Combustors," *Space Propulsion Conference*, 3AF Paper SPC2012_2358097, 2012.

[41] Zhukov, V. P., and Suslov, D. I., "Measurements and Modelling of Wall Heat Fluxes in Rocket Combustion Chamber with Porous Injector Head," *Aerospace Science and Technology*, Vol. 48, Jan. 2016, pp. 67–74. https://doi.org/10.1016/j.ast.2015.10.021

[42] Hardi, J. S., Webster, S. C. L., and Oschwald, M., "Response of a Reacting Cryogenic Oxygen Jet to Transverse Acoustic Forcing," *Space Propulsion 2016*, 3AF Paper SP2016_3124712, 2016.

[43] Sliphorst, M., Gröning, S., and Oschwald, M., "Theoretical and Experimental Identification of Acoustic Spinning Mode in a Cylindrical Combustor," *Journal of Propulsion and Power*, Vol. 27, No. 1, 2011, pp. 182–189. https://doi.org/10.2514/1.49230

[44] Schulze, M., "Linear Stability Assessment of a Cryogenic Rocket Engines," Ph.D. Thesis, Technical Univ. of Munich, Munich, Germany, 2016.

[45] Schulze, M., and Sattelmayer, T., "Linear Stability Assessment of a Cryogenic Rocket Engine," *International Journal of Spray and Combustion Dynamics*, Vol. 9, No. 4, 2017, pp. 277–298. https://doi.org/10.1177/1756827717695281

[46] Urbano, A., Douasbin, Q., Selle, L., Staffelbach, G., Cuenot, B., Schmitt, T., Ducruix, S., and Candel, S., "Study of Flame Response to Transverse Acoustic Modes from the LES of a 42-Injector Rocket Engine," *Proceedings of the Combustion Institute*, Vol. 36, No. 2, 2017, pp. 2633–2639. https://doi.org/10.1016/j.proci.2016.06.042

J. C. Oefelein
Associate Editor